

Odor-Dependent Hemodynamic Responses Measured with NIRS in the Main Olfactory Bulb of Anesthetized Rats

Hyun Joo Lee^{1,5#}, Yunjun Nam^{2#}, Chin Su Koh¹, Changkyun Im¹,
In Seok Seo¹, Seungjin Choi^{2,3,4} and Hyung-Cheul Shin^{1*}

¹Department of Physiology, College of Medicine, Hallym University, Chuncheon 200-702, ²School of Interdisciplinary Bioscience and Bioengineering, ³Division of IT Convergence Engineering and ⁴Department of Computer Science, POSTECH, Pohang 790-784, ⁵Department of Electrical Engineering, University of California, Los Angeles, CA, 90095, USA

In this study, we characterize the hemodynamic changes in the main olfactory bulb of anesthetized Sprague-Dawley (SD) rats with near-infrared spectroscopy (NIRS, ISS Imagent) during presentation of two different odorants. Odorants were presented for 10 seconds with clean air via an automatic odor stimulator. Odorants are: (i) plain air as a reference (Blank), (ii) 2-Heptanone (HEP), (iii) Isopropylbenzene (IB). Our results indicated that a plain air did not cause any change in the concentrations of oxygenated ($\Delta[\text{HbO}_2]$) and deoxygenated hemoglobin ($\Delta[\text{Hbr}]$), but HEP and IB induced strong changes. Furthermore, these odor-specific changes had regional differences within the MOB. Our results suggest that NIRS technology might be a useful tool to identify of various odorants in a non-invasive manner using animals which has a superb olfactory system.

Key words: near-infrared spectroscopy (NIRS), hemodynamic response, main olfactory bulb (MOB), non-invasive, odorant, brain-machine interface (BMI)

INTRODUCTION

An animal's olfactory system is very important for finding food, mating and avoiding predators. These behaviors are initiated by detection and discrimination of odorants in the environment, which involves representation of odorants as unique patterns of neuronal activity in the olfactory system. Previous studies have shown that segregation of sets of functionally similar inputs from olfactory receptor neurons [1, 2] and the postsynaptic outputs of

the dendrites of an exclusive set of mitral/tufted cells. The outputs delineate a mechanism for spatial coding of odors among the MOB neuron ensembles. Many studies have reported this concept of glomeruli as the functional units of spatial code [3-6]. In addition to spatial patterns, both glomerular and mitral/tufted cell activities demonstrate a stimulus-specific temporal structure [7].

Previously, we simultaneously recorded NIRS signals from many single neurons in the anesthetized rats while presenting five different odorants. We found odor-dependent neural responses in the same ensemble of MOB neurons and odor-specific localized differential activation in different regions of the MOB as in McNamara et al's study [8]. We have also reported a method for odorant discrimination based on the maximum likelihood estimation [9]. These results have given us the hope that we

Received December 16, 2010, Accepted March 2, 2011

#These authors equally contributed to this work.

*To whom correspondence should be addressed.

TEL: 82-33-248-2585, FAX: 82-33-248-3426

e-mail: hcshin@hallym.ac.kr

might develop a sensory brain-machine interface (BMI) for the discrimination of valuable chemicals that have odors.

A drawback of an invasive BMI is the problem of immune reaction and inflammation caused when we implant the recording micro-wire electrode in the brain. A potential alternative for an invasive BMI is a non-invasive BMI based on hemodynamic response measurement with near-infrared spectroscopy (NIRS). The NIRS is a method to measure hemodynamic changes due to different absorption of oxy- (HbO₂) and deoxy-hemoglobin (Hbr) via light diffusion in the brain and is useful for investigating brain function for a number of reasons including reasonable cost, high temporal resolution (up to 100 Hz), and portability [10-12]. Therefore, in this study we carried out experiments to test the possibility of discriminating different kinds of smells by measuring hemodynamic responses with a NIRS system in the main olfactory bulb of anesthetized rats. We also tested the possible presence of odor-dependent regional differences of hemodynamic response changes in the MOB.

MATERIALS AND METHODS

Animal preparations

All protocols were approved by the Hallym University Animal Care and Use Committee, and were performed according to the Guide for the Care and Use of Laboratory Animals of the U.S. National Institutes of Health as well as the guidelines of the Animal Welfare Act. Adult Sprague-Dawley (SD) rats (350~400 g, male, n=5) were used in this study. The rats were obtained from the experimental animal center of Orient Bio Co. (linked to the Charles River Lab.). The breeding room environment was

maintained at a temperature of $23\pm 2^{\circ}\text{C}$ and relative humidity of $55\pm 10\%$. Artificial lighting was maintained for 12 hours per day. Two animals were housed in each cage with unlimited food and water. Subjects were anesthetized with i.p. injections of urethane (20%, 1.25 g/kg body weight) and they were transferred to a stereotaxic apparatus and fixed in a prone position. Prior to the surgery and optical recording, we checked their motor responses. After a one-inch middle incision and removal of the skin and soft tissue, the skull was exposed.

We defined the coordinates of the main olfactory (MOB) regions (anterior to posterior: +4.0 mm~+12.0 mm, later to medial: $0\sim\pm 4.0$ mm) from bregma point on the bilateral hemisphere [8].

NIRS and odor-stimulator setup

A commercial sixteen source-channel frequency-domain NIRS system (Imagent, ISS, IL., USA) was used to measure the cerebral hemodynamic responses to olfactory stimulation. This system uses two wavelengths (690 nm, 830 nm), and each channel contains two optical fibers with 400 μm core diameter (FT-400EMT, Thorlabs, NJ, USA) for 690 nm and 830 nm. The optical fibers were arranged as shown in Fig. 1A and a picture of the actual experiment is shown in Fig. 1B. The NIRS channels, source and detector, were separated by 7 mm and the corresponding penetration depth is approximately 2 mm, which is sufficient to cover the cortex area [10]. They encompass both left and right olfactory bulbs. After the optical fibers were placed at appropriate locations, dental cement (KetacCem, 3M, USA) was applied to

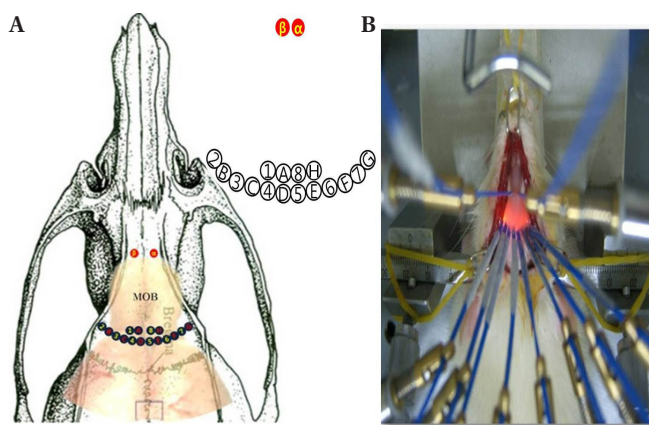


Fig. 1. (A) Arrangement of optical fibers (1~8, A~H are the locations of the source fibers and α , β represent detectors). The main olfactory bulbs (MOB) are located between the detectors and sources. (B) Picture of the actual experiment.

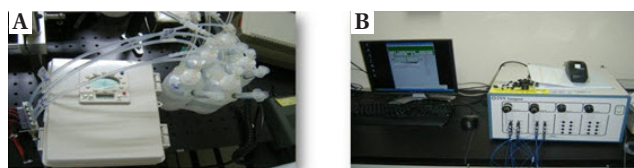


Fig. 2. (A) Motorized odor stimulator with odorant bottles. (B) ISS NIRS system.

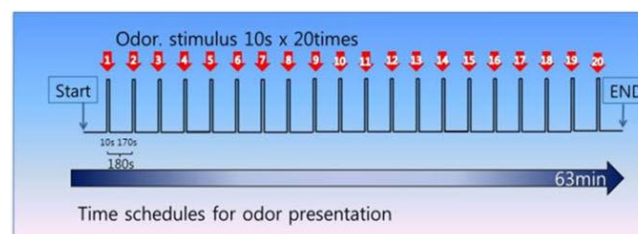


Fig. 3. Time schedules of the experimental procedures. Fastening of the optodes was followed by 120 s of adaptation. Each test epoch consisted of 50 s of baseline followed by 10 s of smell exposure. The protocols of order stimulation were the same in all experiments.

the rat skull to maintain a constant boundary condition between optical fibers and skull [11, 12]. The sampling rate of the NIRS system was 28.4 Hz.

Odorants were diluted with mineral oil to the expected dilution rate (approximately 350 PPM) based on individual odorant vapor pressure. Following the study of Wilson (2008), mixtures were produced by odorant supplements to mineral oil in amounts that provided identical component dilution rates within the mixture [13]. Fig. 2 shows the odor stimulator system and the NIRS system where odorants were delivered by delivered by a motorized odor stimulator and presented 5 mm from the rat's nose for 10 seconds with plain air. The approximate dilution rate was 1 : 1 with plain air. Fig. 3 explains each stimulus was delivered at an interval of about 170 seconds and repeated 20 times for each experiment.

We changed silicone tubes and the bottles containing the odorant each time we used another odorant to prevent unexpected dilution rate. Odorants are: (i) plain air as a reference (Blank), (ii) 2-Heptanone (HEP), (iii) Isopropylbenzene (IB).

Calculation of hemoglobin concentration

We used an analysis program of Boas and Huppert's [14] to calculate cerebral hemodynamic responses. This program provides calculation of ΔHbO_2 and ΔHbr concentration, block average process and image reconstruction. For the recorded intensities from each channel, a modified Beer-Lambert law used to calculate the hemoglobin concentration.

$$\Delta OD^\lambda = -\ln \frac{I_{Final}}{I_{Initial}} = (\epsilon_{HbO_2}^\lambda \Delta[HbO_2] + \epsilon_{Hbr}^\lambda \Delta[Hbr]) B^\lambda L \tag{1}$$

where OD means optical density, I_{Final} is the measured light intensity, and $I_{Initial}$ is the initial light intensity. ϵ is the extinction coefficient of oxy-hemoglobin and deoxy-hemoglobin, and B indicates differential path length factor. λ is the wavelength of light (690 nm and 830 nm). Using this ΔOD^λ , we can obtain ΔHbO_2 (oxy-hemoglobin concentration) and ΔHbr (deoxy-hemoglobin concentration) with the following equations:

$$\Delta[HbO_2] = \frac{\epsilon_{Hbr}^\lambda \frac{\Delta OD^\lambda}{B^\lambda} - \epsilon_{Hbr}^\lambda \frac{\Delta OD^\lambda}{B^\lambda}}{(\epsilon_{Hbr}^\lambda \epsilon_{HbO_2}^\lambda - \epsilon_{Hbr}^\lambda \epsilon_{HbO_2}^\lambda)} L \tag{2}$$

and

$$\Delta[Hbr] = \frac{\epsilon_{HbO_2}^\lambda \frac{\Delta OD^\lambda}{B^\lambda} - \epsilon_{HbO_2}^\lambda \frac{\Delta OD^\lambda}{B^\lambda}}{(\epsilon_{Hbr}^\lambda \epsilon_{HbO_2}^\lambda - \epsilon_{Hbr}^\lambda \epsilon_{HbO_2}^\lambda)} L \tag{3}$$

RESULTS

By using the above protocols, we collected NIRS signals for odor stimuli. Fig. 4 shows representative plots of hemodynamic responses on each channel. The scale of each plot is the "Hbr concentration (AU)"; horizontal axis, "Time (s)": vertical axis and for the representation, while initial level of each signal is set to 0. As shown in the figure, stimuli induced an increase in HbO_2 levels and a decrease in Hbr levels.

Preprocessing and segmentation

To extract clear patterns about hemodynamic responses, signals were low pass-filtered with 0.5 Hz cut-off frequency. Then signals were segmented into two groups: the response state and the relax state. The relax state indicates 20 seconds of signals before chemical stimuli, and the response state indicates of 20 seconds of signals after stimuli. The recorded signals are presented on Fig. 5A. To

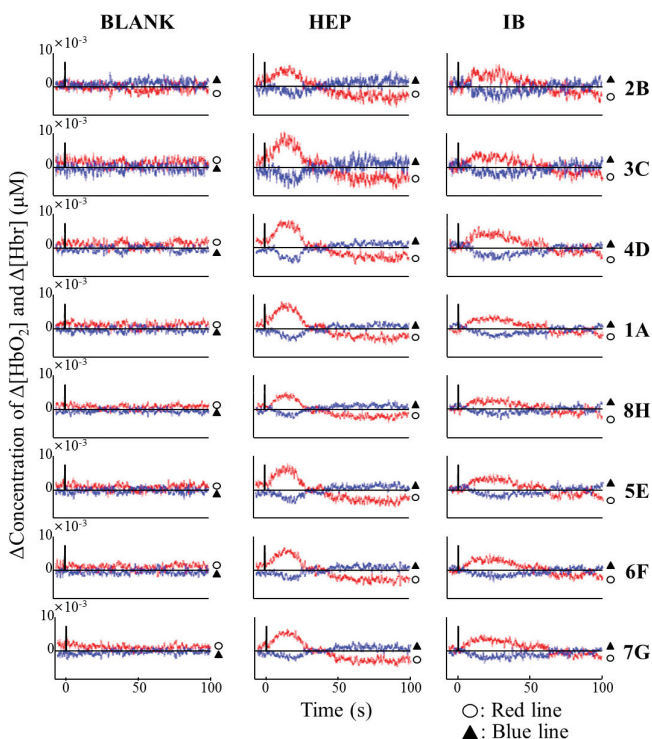


Fig. 4. Representative plots of changes in oxy- and deoxy- hemoglobin concentration when different odors presented. Red and Blue lines indicate change in HbO_2 and HbO_2 concentrations, respectively. Plain air as a reference (Blank), 2-Heptanone (HEP), Isopropylbenzene (IB) from channel 1A to 8H. The graphs show average result of hemodynamic responses to odorants stimulation of one subject (rat no.1018; session4) for 10 s which increased in ΔHbO_2 and decrease in ΔHbr . Each subject showed similar patterns. The ΔHbO_2 concentration was averaged over all subjects and trial sequences. Data were acquired from eight different locations A1, B2 and H8 as demonstrated in Fig. 1, and they showed clear hemodynamic responses.

remove the differences of sensitivity on each channel, the signals were normalized by fixing their variances to 1. Black vertical lines indicate the temporal location of stimuli. When the stimuli is given on time point t , each of the three lines are located on $t-20$, t and $t+20$. So, the time periods between the first and second line belong to the relax state, and periods between the second and third lines belong to the response state. As shown in Fig. 5A, hemodynamic responses for chemical stimuli were observed as a gradual increase of HbO₂ levels and a decreasing of Hbr levels.

Temporal detection

Using these responses, we tried to detect an exact time point of the odor stimuli (t). To increase sensitivity for the detection, we applied Principal Component Analysis (PCA). PCA is a widely used mathematical procedure to find orthogonal basis and it is useful for explaining general shape of data distribution. The method can also be used for extracting linear filters to maximize sensitivity for specific responses. We concatenated all signals in the relax and response states, then found the most principal

component, as follows,

$$w = \arg \max_y (y^T [X_{\text{relax}}, X_{\text{res}}] [X_{\text{relax}}, X_{\text{res}}]^T y),$$

when $X_{\text{relax}}, X_{\text{res}}$ are NIRS signals for relax and response states. A useful characteristic of this component is that it can make distinctive alterations from the stimuli. The filtered signal obtained from $w^T X$ is shown in Fig. 5B. By this process, the signals of 16 channels were transformed into a single channel signal. We could see that the obtained signal shows drastic peaks near the stimuli. However, gradual alteration of the signal's baseline acts as an obstacle for extracting the exact time point of stimuli. To remove this drift, we applied an additional low-pass filter to the signal as shown in Fig. 5C. The time ranges of response states, which we tried to detect, are presented as the red box above the plot. Then by using mean values of relaxes and response states, we calculated the threshold for classification. The threshold is drawn as horizontal dotted line in Fig. 5C. In conclusion, we could successfully detect time periods for response states as shown in Fig. 5D.

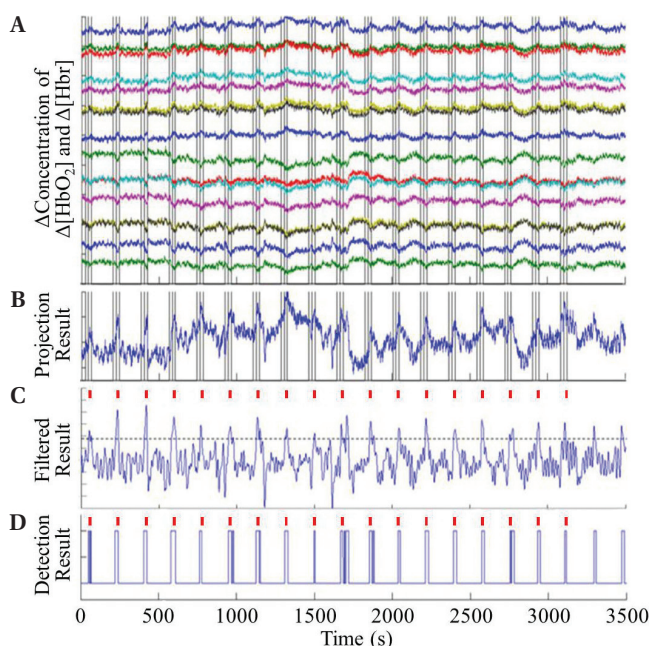


Fig. 5. Temporal detection of odorant stimulation. From band pass-filtered NIRS signals (A), spatial filter w was trained to maximize the sensitivity to the stimuli. By projecting original signals to w we obtained a new one-dimensional signal (B) that shows drastic peaks near the stimuli (indicated as the red box above the plots). To remove drift artifact we applied an additional low-pass filter, then obtained the signal on (C). To detect the exact time point of the stimuli, we applied the threshold value as represented by the blue dashed line on (C). The final detection result is plotted in (D). Time periods predicted as the stimuli are plotted with 1, otherwise 0. We can see that the prediction results is well matched with the actual locations of the stimuli.

Spatial patterns

From the previous analysis, we could extract temporal locations of the stimuli. Our next object was classifying the kinds of odor stimuli. For the classification, we analyzed the spatial patterns of hemodynamic responses. From each trial (a single odor stimuli), we calculated each channel's mean values for relaxes and response states, and measured their differences. So, from a single trial, we obtained a 16-channel data vector. Odor stimuli were repeated 20 times for each kind of odor, and three kinds of odors (HEP, IB and Blank) were continuously given to the rat, as the sequence of Blank, HEP and IB. Then 5 sessions of the above experiment were performed with 5 individual rats. As a result, we collected 300 trials of the difference data vector (20 trials * 3 classes * 5 sessions) and made the difference data matrix $X \in \mathbb{R}^{16 \times 300}$. To fulfill our object, the classification of odorants, we re-segmented X into $X_{\text{blank}}, X_{\text{HEP}}$ and X_{IB} , and compared each of them.

Fig. 6 shows the analysis results for the experiment of 4th session of the experiment. From X , we extracted only the data vectors belonged to session 4, and put that data as matrix $X_{(4)} \in \mathbb{R}^{16 \times 60}$. Then $X_{(4)}$ segmented to $X_{\text{blank}(4)}, X_{\text{HEP}(4)}$ and $X_{\text{IB}(4)}$.

Fig. 6A shows a comparison results between $X_{\text{HEP}(4)}$ and $X_{\text{blank}(4)}$. At first, we calculated mean values $X_{\text{HEP}(4)}$ and $X_{\text{blank}(4)}$ then showed their differences on the table on the right side. As already explained, hemodynamic responses for olfactory stimuli are observed as increased HbO₂ levels with decreased of Hbr levels. Results of the table fit well with the phenomena. The results also presented as

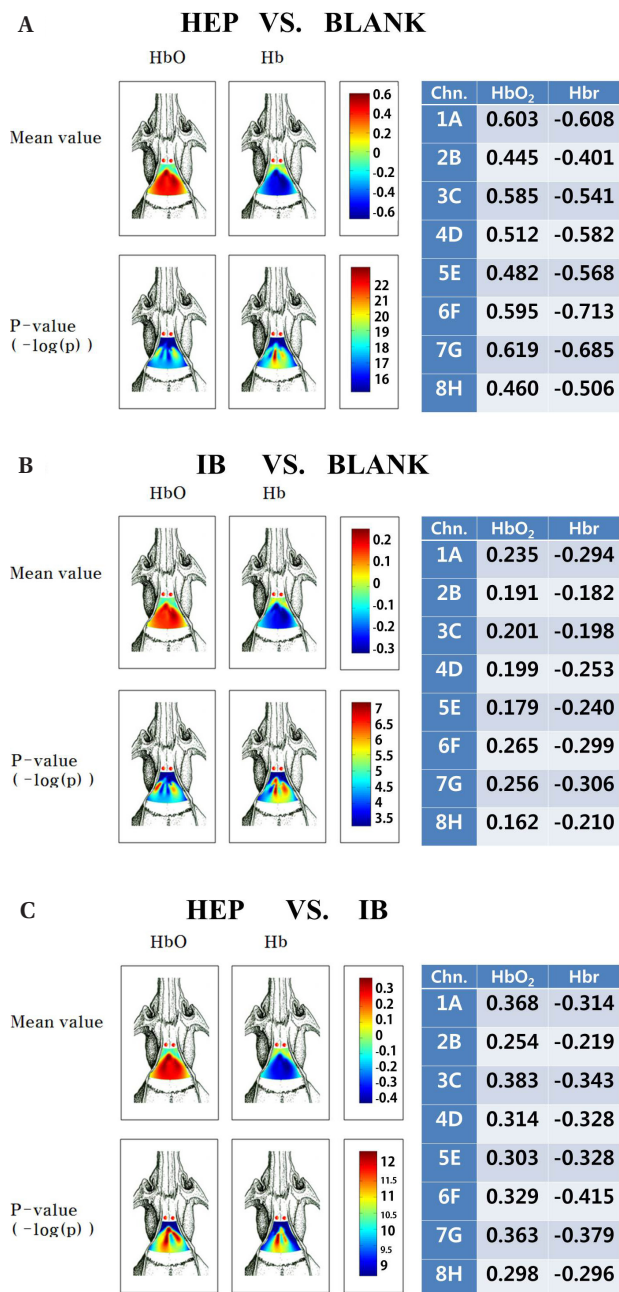


Fig. 6. Comparison of spatial patterns for session 4. (A) Comparison between HEP and Blank. (B) Comparison between IB and Blank. (C) Comparison between HEP and IB.

topoplots on the left side. The plots show that the differences of channel 1A and 6F are more significant than other channels.

To investigate the possibility of the classification, we performed a *t*-test between $X_{HEP(4)}$ and $X_{blank(4)}$, then drew topoplots of the bottom row based on its results. The p-values obtained from two-sample *t*-test are finer measures than simple difference to prove discriminativeness between groups. It considers not only differences of means, but also variances, which are closely related

to overlapping between groups. On the *t*-test, smaller p-values mean that the difference is relatively larger. So, to intensify the regions with smaller p-values, we applied a $-\log$ function on p-values and drew the topoplots by the values. Unlike upper-row mean value-based plots, 2B, 7G of HbO₂ levels and 4D of Hbr levels showed more significant differences on p-value based plots.

The same kind of analysis performed between $X_{IB(4)}$ and $X_{blank(4)}$ as shown in Fig. 6B. Trends of HbO₂ and Hbr levels are observed quite often with Fig. 6A, as shown on the table and upper plots. Furthermore, HEP and IB shares similar spatial patterns. Mean value-based plots also indicates 1A and 6F as discriminative channels like Fig. 6A and p-value based plots point to 2B, 7G (in HbO₂) and 4D (in Hbr) as informative channels. Although 1A and 6F more significantly emphasized on Hbr levels of p-value analysis, general patterns showed similar shapes. However, magnitudes of alteration showed clear difference between HEP and IB. The differences caused by IB were smaller than the results of HEP. The difference caused by HEP stimuli caused HbO₂ levels to vary from 0.445 to 0.619 (mean value=0.538) and -0.713 to -0.401 (mean value= -0.576) on Hbr levels, but IB showed value range of 0.162~0.265 (mean value=0.211) and -0.306 ~ -0.182 (mean value= -0.247). Because of these small differences, p-value also showed a higher value range of 10^{-7} ~ $10^{-3.5}$.

From the above two analyses, we observed that the hemodynamic alteration caused by HEP and IB share similar patterns but their magnitude is different. In the third step of analysis, we compared $X_{HEP(4)}$ and $X_{IB(4)}$ as shown in Fig. 6C. This analysis is more important in practical terms than the previous two analyses, because it is directly related to the classification of odors.

The results in the table were calculated by $\text{mean}(X_{HEP(4)}) - \text{mean}(X_{IB(4)})$. Because of $X_{HEP(4)}$ has larger value ranges than $X_{IB(4)}$, values for HbO₂ levels have a positive range and values for Hbr have a negative range. p-value based plots extract 1A, 4D and 7G (on HbO₂) and 4D and 8H (on Hbr) as the discriminative channels. These results are slightly different from the previous two comparisons. This difference implies that even though the direction of hemodynamic alteration by HEP and IB is similar, there is a subtle difference between them, and it could be beneficial for following classifications.

We extended the above analysis to the entire data set X from 5 sessions as shown in Fig. 7. The results were not much different to those in Fig. 6. The stimuli increased HbO₂ levels and decreased Hbr levels. HEP caused more significant response than IB. Mean value-based topoplots showed similar results to Fig. 6, but p-value based topoplots showed slightly different results because data from different rats were mixed.

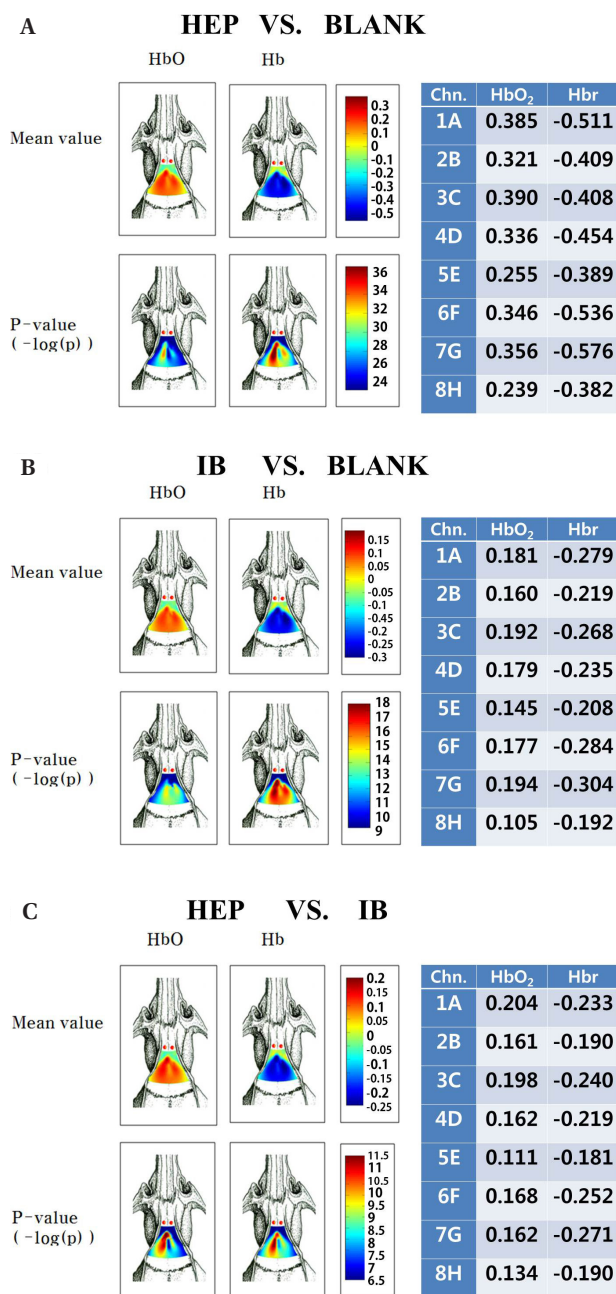


Fig. 7. Comparison of spatial patterns for all data including 5 sessions. (A) Comparison between HEP and Blank. (B) Comparison between IB and Blank. (C) Comparison between HEP and IB.

Classification

By the above analysis, we confirmed that the classification of each odor stimuli could be possible. As the final step of the analysis, we tried classification of signals. At first, we attempt the classification between relax signals (X_{blank}) and response signals (X_{HEP} , X_{IB}). For the classification, we used the linear-kernel based SVM (Support Vector Machine) method. To evaluate classification performances, we performed 5-fold cross validation test. We calculated the test

Table 1. Classification result for Blank vs. Stimuli (IB+HEP)

Session	Session 1	Session 2	Session 3	Session 4	Session 5
Accuracy (%)	74.7	88.9	74.1	87.0	64.8

Table 2. Classification result for IB vs. HEP (%)

Session	Session 1	Session 2	Session 3	Session 4	Session 5
Accuracy (%)	83.3	72.2	61.1	91.7	66.7

for each session, and the results are presented in Table 1. The performance fluctuated sharply between sessions from 64.8% (session 5) to 88.9% (session 4).

Secondly, we performed classification between odorant responses for two different stimuli. As already explained in the previous subsection, the difference between X_{HEP} and X_{IB} is smaller than the difference between relax and response signals. To overcome this lesser discriminability, we applied RBF (radial basis function) kernel-based SVM for the classification.

For the classification of each session, we tried both linear kernel and RBF kernel-based classification approaches, and we show best results in Table 2. In the first session and the third session, RBF kernel was used and in other sessions, linear kernel was used. The mean accuracy of the classifying stimuli was 77.9%, while the mean accuracy of odor classifications was 75.0%. 77.9% and 75.0% may not be satisfactory scores from the viewpoint of interface research. However, we confirmed that the magnitude of hemodynamic response from two different odor stimuli is significantly different, and sometimes it enables plausible accuracy of the classification as shown in the result of the session 4. We also observed subtle differences of spatial patterns between two responses on the t -test. These aspects of spatial patterns differences imply that improved measuring device/techniques and sophisticated classification algorithms can enhance the performance of the BMI system.

DISCUSSION

The main goal of this study was to use the NIRS system to record activity in the olfactory bulb. As mirrored by changes in blood flow during presentation of chemical odorants as well as spicy fruit (HEP), aromatic smell (IB) and plain air (Blank), respectively.

The NIRS system has several advantages specifically it is non-invasive, not painful and confers no exposure to harmful light sources. Previously studies with functional magnetic resonance imaging (fMRI) in adults have shown that olfactory stimulation activates a number of different regions of the brain [15-17].

Previously NIRs studies just focused on results of fMRI or PET studies during motor, visual and cognitive experiments [18-21]. However, in recent years, NIRs has become useful systems in mapping the brain during dynamic experiments. We have obtained a significant result by investigating the change of hemodynamic responses in the olfactory regions of an animal's brain.

Our study confirmed that NIRS were able to measure the specific hemodynamic responses of the brain during the presentation of various odors. The responses were from the MOB of anesthetized rats in experiments. Here we wish to point out that the method of similar study that was previously carried out the difference pattern of neuron spikes from MOB via invasive method to the odor discrimination.

The alterations of hemodynamic responses caused by HEP, aromatic smells (perceived by adults as a spicy fruity smell) were 2.2 times greater than IB (perceived by adults as an aromatic smell) but those alterations were stronger than the response the plain air. It might be tempting to explain this in terms of quantitative differences in emitted molecules and hence in the number of odor receptors engaged or the intensity of the inactivation [22].

We showed topoplots that reflected the regional basic activation patterns of olfactory bulbs during presentation of various odors in rodents. And through recorded raw data we can inferred the time when stimuli presented during the experiment session. Each of these results is very interesting as a scientific research.

Hence further studies are needed to delve into the influence of other experimental parameters, such as the number of stimuli, rate of dilution, order of stimuli, kinds of odorant on hemodynamic responses on olfactory bulbs. In this study, we presented from 18 to 20 times odor stimuli (total n; 5 rats, 90~100 times odor stimuli/each rat) to measure hemodynamic responses. Further studies should also investigate the number of stimuli and the discrimination accuracy with multivariate autoregressive (MVAR) modeling method called "Granger causality". According to Schlogl's study [23], the accuracy of the MVAR estimation is somewhat dependent on the number of time samples and the variance of the prediction error becomes smaller than 10% of the signal variance if the number of samples is larger than 70. The topoplots could provide more chance for the understanding brain activities such as hemodynamic responses that in odor stimuli tasks using NIRs. This is also of interest in connection with the specific brain region while presenting various stimuli such as music, decision making problems, or video games.

This experiment is intended to yield results that can be applied to develop a prototype BMI system for olfactory discrimination from brain blood changes, recorded either electro-physiological

or optical (NIRS) methods. And practical applications of the olfactory sensory BMI could be used for various scent industries.

ACKNOWLEDGEMENTS

This work was supported by NRF (2011-0018283, 2011-0018284) to SJCHOI, NRF (2010-355-H00003) to HJLEE, BRC (2011K000284), MKE (10033634-2011-13) & NRF (2009-0094073, 20110018285) to HCSHIN.

REFERENCES

1. Buck L, Axel R (1991) A novel multigene family may encode odorant receptors: a molecular basis for odor recognition. *Cell* 65:175-187
2. Mombaerts P (1999) Molecular biology of odorant receptors in vertebrates. *Annu Rev Neurosci* 22:487-509
3. Bozza T, Vassalli A, Fuss S, et al (2009) Mapping of class I and class II odorant receptors to glomerular domains by two distinct types of olfactory sensory neurons in the mouse. *Neuron* 61: 220-233
4. Guthrie KM, Anderson AJ, Leon M, Gall C (1993) Odor-induced increases in c-fos mRNA expression reveal an anatomical "unit" for odor processing in olfactory bulb. *Proc Natl Acad Sci US A* 90:3329-3333
5. Johnson BA, Ho SL, Xu Z, et al (2002) Functional mapping of the rat olfactory bulb using diverse odorants reveals modular responses to functional groups and hydrocarbon structural features. *J Comp Neurol* 449:180-194
6. Wachowiak MP, Smolliková R, Zheng Y, Zurada JM, Elmaghraby AS (2004) An approach to multimodal biomedical image registration utilizing particle swarm optimization. *IEEE Trans Evol Comput* 8:289-301
7. Meredith M (1986) Patterned response to odor in mammalian olfactory bulb: the influence of intensity. *J Neurophysiol* 56: 572-597
8. McNamara AM, Cleland TA, Linster C (2004) Characterization of the synaptic properties of olfactory bulb projections. *Chem Senses* 29:225-233
9. You KJ, Ham HG, Lee HJ, et al (2011) Odor discrimination using neural decoding of the main olfactory bulb in rats. *IEEE Trans Biomed Eng* 58:1208-1215
10. Crespi F, Bandera A, Donini M, Heidbreder C, Rovati L (2005) Non-invasive in vivo infrared laser spectroscopy to analyse endogenous oxy-haemoglobin, deoxy-haemoglobin, and blood volume in the rat CNS. *J Neurosci Methods* 145:11-22
11. Lee S, Koh D, Kwon K, et al (2009) Hemodynamic responses

- of rat brain measured by near-infrared spectroscopy during various whisker stimulations. *J Opt Soc Korea* 13:166-170
12. Lee S, Lee M, Koh D, Kim BM, Choi JH (2010) Cerebral hemodynamic responses to seizure in the mouse brain: simultaneous near-infrared spectroscopy-electroencephalography study. *J Biomed Opt* 15:037010
 13. Barnes DC, Hofacer RD, Zaman AR, Rennaker RL, Wilson DA (2008) Olfactory perceptual stability and discrimination. *Nat Neurosci* 11:1378-1380
 14. PMI Lab-HomER [Internet]. Available from: <http://www.nmr.mgh.harvard.edu/PMI/resources/homer/home.htm>
 15. Fulbright RK, Skudlarski P, Lacadie CM, et al (1998) Functional MR imaging of regional brain responses to pleasant and unpleasant odors. *AJNR Am J Neuroradiol* 19:1721-1726
 16. Levy LM, Henkin RI, Hutter A, Lin CS, Martins D, Schellinger D (1997) Functional MRI of human olfaction. *J Comput Assist Tomogr* 21:849-856
 17. Sobel N, Prabhakaran V, Desmond JE, et al (1998) Sniffing and smelling: separate subsystems in the human olfactory cortex. *Nature* 392:282-286
 18. Hirth C, Obrig H, Villringer K, et al (1996) Non-invasive functional mapping of the human motor cortex using near-infrared spectroscopy. *Neuroreport* 7:1977-1981
 19. Takahashi K, Ogata S, Atsumi Y, et al (2000) Activation of the visual cortex imaged by 24-channel near-infrared spectroscopy. *J Biomed Opt* 5:93-96
 20. Watanabe E, Maki A, Kawaguchi F, et al (1998) Non-invasive assessment of language dominance with near-infrared spectroscopic mapping. *Neurosci Lett* 256:49-52
 21. Watanabe E, Yamashita Y, Maki A, Ito Y, Koizumi H (1996) Non-invasive functional mapping with multi-channel near infra-red spectroscopic topography in humans. *Neurosci Lett* 205:41-44
 22. Winberg J, Porter RH (1998) Olfaction and human neonatal behaviour: clinical implications. *Acta Paediatr* 87:6-10
 23. Schlögl A (2006) A comparison of multivariate autoregressive estimators. *Signal Processing* 86:2426-2429